J Mater Sci (2007) 42:2334–2346
DOI 10.1007/s10853-007-1592-z

TEM microstructural analysis of As-Bonded Al–Au wire-bonds

Adi Karpel · Giyora Gur · Ziv Atzmon · Wayne D. Kaplan

Received: 20 January 2007 / Accepted: 7 February 2007 / Published online: 12 March 2007
© Springer Science+Business Media, LLC 2007

Abstract In this study the interface morphology of a model 99.999% (5N) Au wire bonded to Al pads in the as-bonded state was examined by scanning/transmission electron microscopy with energy dispersive spectroscopy. Specimens for transmission electron microscopy were prepared using the lift-out method in a dual-beam focused ion beam system. Analysis of the bond microstructure was conducted as a function of the Al pad content and as a function of the bonding temperature. Additions of Si and Cu to the Al pad affect the morphology and the uniformity of the interface. A characteristic-void line is formed between two intermetallic regions with different morphologies in the as-bonded samples. According to the morphological analysis it was concluded that a liquid phase forms during the bonding stage, and the void-line formed in the intermetallic region is the result of shrinkage upon solidification and not the Kirkendall effect.

Introduction

Wire-bonding is the one of the key industrial techniques to connect semiconductor devices to the macroscopic circuit arranged on a circuit board [1]. Wire-bonding provides an electric connection, for example, of an aluminum pad on a silicon die to a lead frame. The most commonly used system is high-purity Au 99.99% (4N) wires bonded to Al pads. A combination of thermal and ultrasonic energies is employed to form a bond between the Au wire and the Al pad, as well as between the wire and the lead frame [1]. Given the nominally low-temperature process (usually in the range of 120–240 °C), it is usually assumed that the bond is formed in the *solid* state via the formation of intermetallics by solid-state diffusion [1].

During the wire bonding process an interface region that is composed of Al and Au is formed [1–6]. Previous studies have shown that Al–Au intermetallics are formed during the bonding stage and during the subsequent packaging processes [7]. The Al–Au intermetallics that were found to form during wire-bonding and packaging processes of Au wire to *pure* Al pads are the thermodynamically stable Al–Au intermetallics [2, 4, 6]. In order to increase the electromigration resistance of the Al pad, Si and Cu are added [1]. The Si–Cu additions reduce the uniformity of the intermetallic coverage, and can influence which intermetallics are formed during the bonding process [6–8].

The Al–Au intermetallic region of the bond contains flaws in the form of voids. Previous studies of the morphology of the interface region that is formed at the bonding stage suggested that the flaws result from contaminates and residual native oxide layers that formed prior to bonding. The oxide layers are believed to prevent complete contact between the Au ball bond and the Al pad [2–5]. Other studies have suggested that during the life-time of the device, growth of the

A. Karpel · W. D. Kaplan (✉)
Department of Materials Engineering, Technion—Israel Institute of Technology, Haifa 32000, Israel
e-mail: kaplan@tx.technion.ac.il

G. Gur · Z. Atzmon
Kulicke & Soffa Bonding Tools, Yokneam Elite 20692, Israel

intermetallic region occurs by diffusion, and due to the different diffusion rates of Au and Al in the intermetallic phases, voids form in the intermetallic region (Kirkendall effect) [3–6, 9, 10]. However, the size and distribution of voids does not correlate with the characteristic morphology associated with the Kirkendall effect.

Previous analysis of wire-bonds has been mostly done using energy dispersive spectroscopy (EDS) combined with scanning electron microscopy (SEM) [1–6]. The main disadvantage of this technique for the characterization of Au–Al wire-bonds is the relatively large volume of interaction which defines the source of the EDS signal. The size of the interaction volume can exceed the grain size of the Al–Au intermetallics at the interface between the Au wire and Al pad, which reduces the accuracy of the results [11].

SEM-EDS analysis does not usually provide information on the *crystallographic* structure of the Al-Au intermetallic region that is formed during the wire-bonding process, which in turn can have a significant effect on volume changes and residual stresses. In addition, flaws that are formed during phase transformations in the bonding stage continue to evolve during the life-time of the device, and can lead to device failure. Therefore, in order to understand and prevent failure that occurs during the life-time of the device, it is important to understand the microstructure that is formed during the initial ball-bonding stage of the wire-bonding process. This kind of analysis can be done using transmission and scanning transmission electron microscopy (TEM and STEM) combined with EDS analysis of thin foils, which due to the smaller electron beam diameter and interaction volume has a better spatial resolution than SEM-EDS [11].

The main problem with TEM/STEM analysis of wire-bonds is specimen preparation, which demands site-specific analysis. In addition, conventional specimen preparation can result in mechanical damage of the interface region during polishing. These problems can be overcome by using a dual-beam focused ion beam (FIB) system, which combines scanning electron microscopy (SEM) with a scanning ion beam [12]. In this way specific regions can be located using SEM and SEM/TEM specimens prepared without the application of mechanical forces. The goal of this study was to understand the processes that result in the initial formation of an intermetallic region during the ball-bonding stage of the wire-bonding process by applying advanced electron microscopy techniques.

Experimental

Materials

Si wafers were diced and die attached prior to wire bonding. Bonding was performed with a 120 kHz Kulicke & Soffa model 8028 PPS automatic wire bonder. A 17.8 μm diameter Au wire of 99.999% purity (5N) was used for wire bonding on an ink die with 1 μm thick Al pads deposited on a thermally grown SiO_2 layer. Two kinds of Al pads were examined: Al–1.0 wt.%Si and Al–0.1 wt%Si–0.5%Cu.

For subsequent characterization of the morphology of conventionally wire-bonded samples, thermosonic ball bonding of each Si die was performed at 165 °C for an average time of less than ~30 s for each device, with a maximum preheat and post-heat time of ~45 s at 150°C. The ball bond diameter was kept within 31 ± 2 μm. The bonding parameters were optimized and checked using a ball shear test [1, 13]. The resultant average bond shear force was 7.2 g.

The total time for each bond was ~140 ms. The time for each of the steps in the bonding process, as schematically described in Fig. 1, is as follows: free air ball (FAB) formation of a Au ball by an electrical spark required ~10–20 ms; the time to produce both the first bond (on the Al pad) and the second bond (on the lead frame) was ~20–30 ms with ~60–70 ms to extend the wire between the pad and the lead (loop-time).

In order to analyze the microstructure formed only during the application of ultrasonic energy and temperature, a series of wire-bonds was prepared at 120 kHz. The temperatures of the pre and post bonding sites were kept at 30 °C, and the temperature of each die during the wire-bonding process was set at a constant (known) temperature between 30 and 215 °C. The die temperature was verified by direct measurement using a thermocouple.

A 17.8 μm diameter Au wire of 99.999% purity (5N) was used for wire bonding on a test die with a 1 μm thick Al–0.1 wt%Si pad deposited on thermally grown SiO_2. The bonding parameters that were investigated were the bond diameters and the shear force as a function of the bonding temperature. The shear force was analyzed by the ball shear-test and the sample size was 20 bonds in each die. During the wire-bonding process the die is exposed to the bonding temperature. This can result in additional diffusion processes in the bonded regions. Therefore, in order to understand the morphology that is formed only during application of the ultrasonic energy and temperature, S/TEM samples were prepared from the very last bonded region on the die.

Characterization

The shear strength of the wire-bonds was measured using a Dage4000 shear tester, using lateral movement (parallel to the plane of the wafer) of a shear tool positioned near the bond. The maximum shear value was measured by a strain gauge transducer [1, 13].

The TEM samples were prepared from the wire-bonded samples using the lift-out technique [12]. One of the advantages of the dual-beam FIB is that no mechanical force is applied during sample preparation, and the analyzed region can be chosen using the SEM mode of the system. The Au wires were cut using the ion beam at a high current (21nA and 30 kV). A thin lamella was prepared by rough milling (21 nA), followed by additional milling at a lower current (0.28 nA) to clean the surface of the cross-section from redeposition that occurs during rough milling. The lamella was attached to a W needle by Pt deposition using a gas injection system, detached from the Si die by ion milling and attached to a Mo grid by Pt deposition. At this stage additional thinning was conducted at a low current (28–93 pA) in order to achieve the thickness required for TEM. The thickness was monitored during thinning with a high angle annular dark field (HAADF) STEM detector mounted in the FIB. Thinning was stopped when regions in the sample that contained high atomic number elements (e.g. Au) generated a bright contrast in the HAADF-STEM images [11].

Conventional TEM analysis was done at 200 kV (JEOL 2000FX including a Thermo Noran super-thin window Si(Li) EDS). Analytical TEM was conducted using a Tecnai F20 G^2 field emission gun (FEG) TEM, equipped with a HAADF STEM detector, operated with a beam diameter of ~1 nm and a retractable EDS (EDAX Energy Dispersive X-Ray Spectrometers with sapphire Si(Li) detectors).

EDS analysis was conducted in two modes depending on the size of the analyzed region; EDS acquisition while the electron beam was rastered over a defined region, and point EDS analysis using ~1 nm diameter electron beam. EDS quantification was done using the Cliff-Lorimar approximation and calculated standards, leading to ~20% error.

Results

Morphology of conventional bonds

The Al pads that are used for the wire-bonding process usually contain Si and Cu in order to increase their

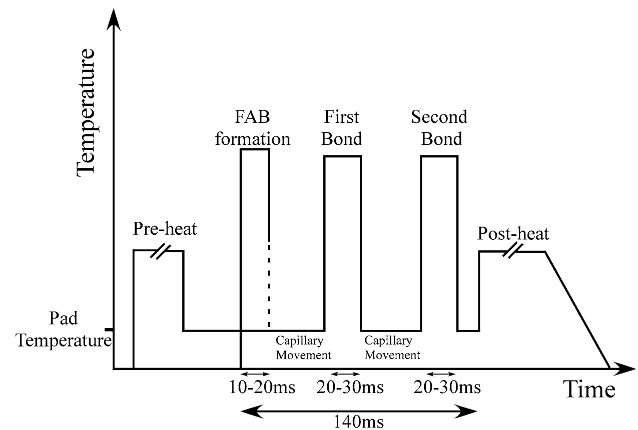

Fig. 1 Schematic drawing of the different stages of wire bonding process used to prepare samples in the present study

resistance to electromigration. This also results in morphological changes of the Al-Au intermetallics that are formed during the wire-bonding process [6]. In this study the morphology of wire-bonding of 5N Au wire to Al–1.0wt.%Si and Al–1.0wt.%Si–0.5wt.%Cu was analyzed.

Bonding to A1–1.0wt.%Si pads

Figure 2 is a bright field (BF) diffraction contrast TEM micrograph of the interface region of a bond between a 5N Au wire and a Al–1.0wt.%Si pad. Intermetallics were formed during the bonding process, containing four distinct regions with different morphologies: The region indicated as I is a thin layer with no distinct

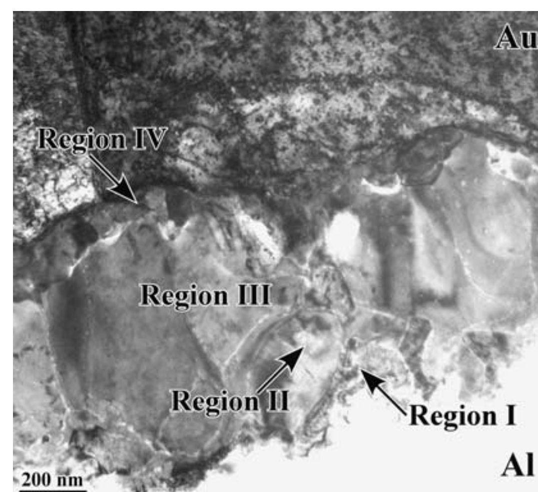

Fig. 2 BF TEM micrograph presenting the morphology of the interface region of a bond between the Au wire and a Al–1.0wt.%Si pad. The Al pad has a white contrast, due to it's relatively low mass-thickness compared to Au

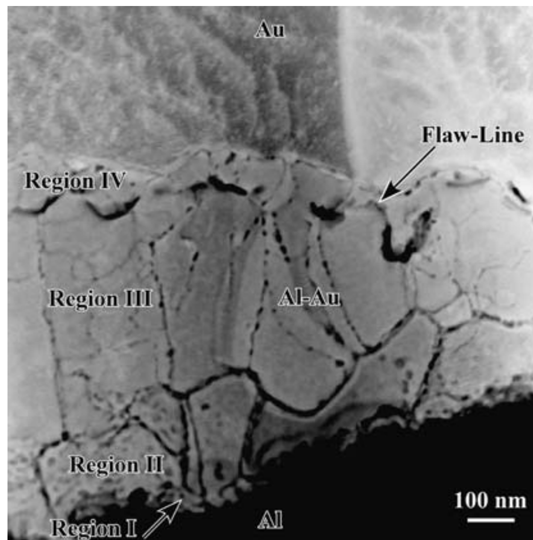

Fig. 3 HAADF STEM micrograph of the interface region of the bond between a Au wire and a Al–1.0wt.%Si pad, showing the intermetallic region which contains a relatively high density of fine voids

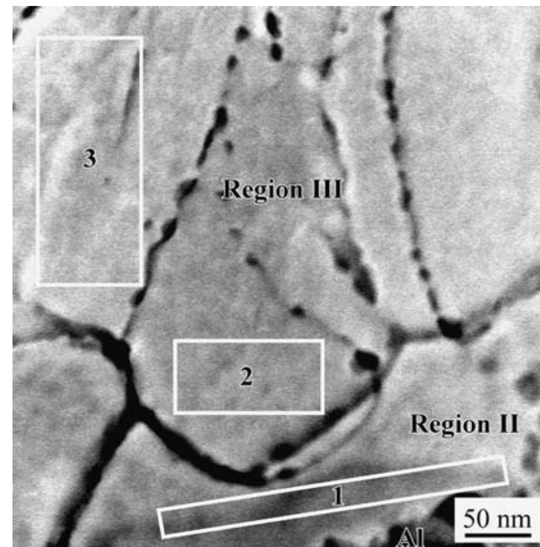

Fig. 4 HAADF STEM micrograph of regions II and III in the bond between a Au wire and a Al-1.0wt.%Si pad. EDS analysis was conducted in the indicated regions

morphology; region II contains small elongated grains; region III contains elongated anisotropic grains; and region IV is a thin layer containing small almost equiaxed grains. Regions III and IV are separated by a line of flaws in the form of voids. The grain boundaries of the intermetallic grains contain a high density of small voids. The Au grains adjacent to the Al–Au layer contain a high density of small dislocation loops caused by Ga^{+} ion radiation damage during TEM sample preparation by FIB [14].

Figure 3 is a HAADF STEM micrograph of the Al–Au intermetallic region. In this imaging mode mass-thickness contrast is dominant. Therefore, a brighter contrast is obtained from regions with a larger mean atomic number [11]. The difference between the atomic number of Au and Al results in large contrast changes between the Al and the intermetallics, and in the black contrast from the residual Al pad. The four different regions that were identified in Fig. 2 are also visible in Fig. 3. The dark contrast at the grain boundaries in Fig. 3 results from the high density of flaws in the form of voids. Voids are also located inside some of the intermetallic grains. Region II also contains a high density of voids. The BF TEM micrograph in Fig. 2 showed that region IV is separated from region III by a line of voids. HAADF STEM (Fig. 3) showed that voids are also present between region IV and the Au adjacent to the intermetallic region.

Figure 3 demonstrates the relatively high density of fine voids that are formed *during* the wire-bonding process. The time required to form the bond is ~20–30 ms, and the total time of heating is ~2 min, which is insufficient for void formation by the Kirkendall phenomenon.

In order to understand if the morphological changes are the result of compositional changes, EDS analysis was conducted on the regions indicated on the HAADF STEM micrograph in Fig. 4, and the results are presented in Table 1, indicating that during the bonding process Au-rich intermetallic phases are formed.

Due to the small size of regions I and IV, EDS point analysis was conducted on the regions indicated in the HAADF STEM micrographs presented in Figs. 5 and 6. The results of the EDS analysis from region IV are summarized in Table 2, which indicates that the amount of Au in region IV is greater than in region III, signifying that the void-line between region III and IV is a border between two regions with a different composition.

The results of the EDS analysis of region I are summarized in Table 3. The compositional changes that are presented could result from drift of the specimen and/or the electron beam during EDS analysis. According to the EDS results from points 2 and 3, the

Table 1 EDS results of areas 1–3 in Fig. 4

	1	2	3
Al (K) [at.%]	20 ± 4	12 ± 3	12 ± 3
Au (L) [at.%]	76 ± 11	83 ± 12	87 ± 13
Si (K) [at%]	4 ± 1	4 ± 1	1 ± 0.2

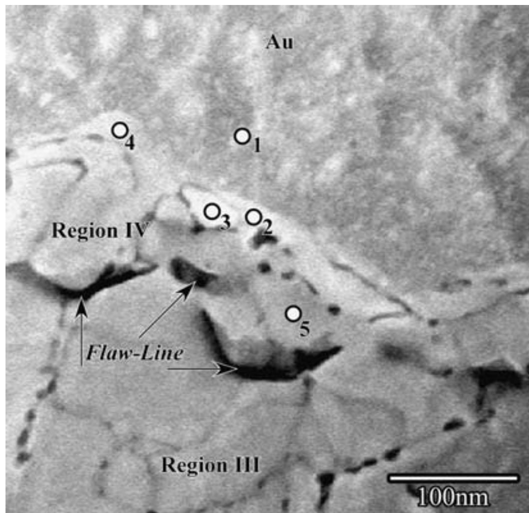

Fig. 5 HAADF STEM micrograph of the bond between a Au wire and a Al–1.0wt.%Si pad. EDS analysis was conducted at the marked points

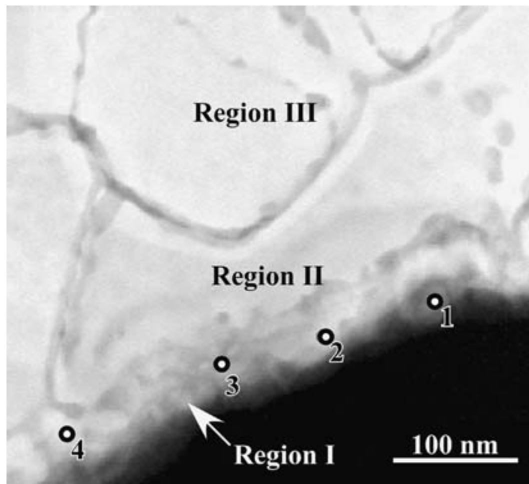

Fig. 6 HAADF STEM micrograph of the bond between a Au wire and a Al–1.0wt.%Si pad. EDS analysis was conducted at the marked points

Table 2 EDS results of points 1–5 in Fig. 5

	1	2	3	4	5
Al (K) [at.%]	0	3 ± 1	6 ± 1	7 ± 1	10 ± 2
Au (L) [at.%]	96 ± 15	69 ± 15	96 ± 13	88 ± 13	88 ± 13
Si (K) [at.%]	3 ± 0.6	1 ± 0.2	4 ± 1	4 ± 1	2 ± 0.4

middle of region I contains almost equal amounts of Al and Au.

The structure of the intermetallics in region III was analyzed by selected area electron diffraction (SAD). Figure 7a is a BF TEM micrograph of the Al–Au intermetallic region, where the indicated grain in region III is in a low-index zone axis. The SAD from the indicated grain presented in Fig. 7b confirms the Al_3Au_8 hexagonal structure in a $[13\bar{4}1]$ zone axis (see appendix).

Table 3 EDS results of points 1–4 in Fig. 6

	1	2	3	4
Al (K) [at.%]	63 ± 13	43 ± 9	44 ± 9	23 ± 8
Au (L) [at.%]	32 ± 6	52 ± 8	51 ± 8	75 ± 11
Si (K) [at.%]	2 ± 0.4	3 ± 1	2 ± 0.4	2 ± 0.4

Bonding to Al–1.0wt.%Si–0.5wt.%Cu pads

Figure 8 presents a HAADF STEM micrograph of the interface region of a bond between a 5N Au wire and a Al–1.0wt.%Si–0.5wt.%Cu pad. A relatively high dislocation density is present in the Au region adjacent to the intermetallics and to the Al pad, which can be seen due to residual diffraction contrast in the HAADF STEM micrograph. Islands of intermetallics are located along the interface, alongside Au regions that did not react with the Al. Void-lines are present inside the intermetallic islands, and in addition, voids exist between the Au regions and the intermetallic islands. This suggests that shrinkage occurs upon the formation of the Al–Au intermetallics. Regions where no reaction occurred between the Al and the Au have a smooth morphology compared to the reacted region. A comparison of the interface between the Au and Al and the interface between the intermetallics and the Al pad suggest that most of the intermetallic region is formed inside the Au region.

EDS analysis was conducted on the areas indicated in Fig. 9. The results are presented in Table 4. Si and Cu are present in all of the analyzed regions, which can stabilize Al–Au intermetallics that are not present in the Al–Au binary equilibrium phase diagram. A detectable decrease in Al content in the intermetallics is found when bonding Au to a Al–0.1wt.%Si pad compared to a Al–0.1wt.%Si–0.5wt.%Cu pad.

Figure 10a presents a BF TEM micrograph of the intermetallic region seen in Fig. 8. Two SADs in different zone axes were taken from the marked grain in region II, and are presented in Figs. 10b and c. Both SADs confirms the existence of the metastable cubic form of $AlAu_4$ [15] (see appendix). According to these results it can be understood that the presence of Si and Cu in the Al pad affects the intermetallics that are formed during the wire-bonding process.

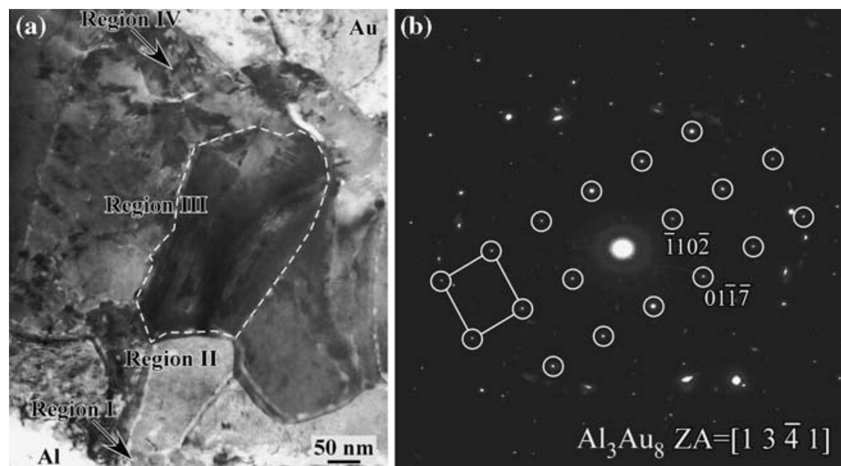

Fig. 7 (**a**) BF TEM micrograph of the intermetallic region of a Au wire bonded to a Al–1.0wt.%Si pad. The grain indicated by a dashed line in (**a**) is Al_3Au_8, which was confirmed by the SAD presented in (**b**)

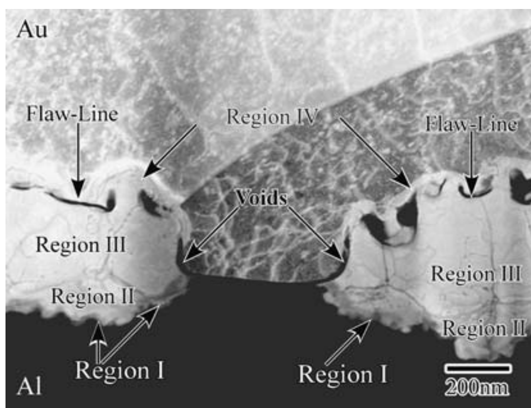

Fig. 8 HAADF STEM micrograph of the interface between a Au wire and a Al–1.0wt.%Si–0.5 wt%Cu pad, presenting the formation of a non-uniform intermetallic region that contains voids

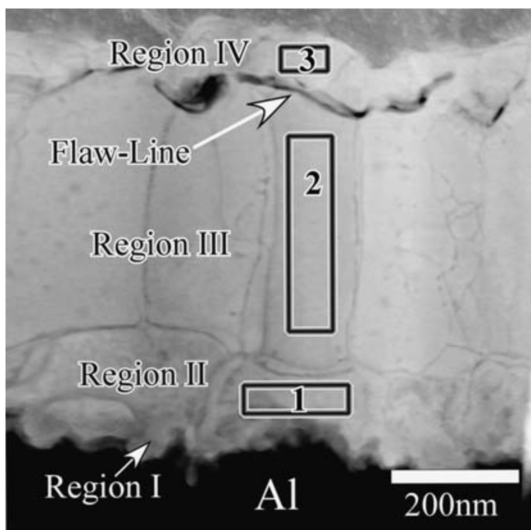

Fig. 9 HAADF STEM micrograph of the interface between a Au wire and a Al–1.0wt.%Si–0.5 wt%Cu pad. EDS analysis was conducted on the indicated areas

Table 4 EDS results from the areas marked as 1–3 in Fig. 9

	1	2	3
Al (K) [at.%]	14 ± 3	10 ± 2	9 ± 2
Au (L) [at.%]	83 ± 13	84 ± 13	85 ± 13
Si (K) [at.%]	3 ± 1	3 ± 1	4 ± 1
Cu (K) [at.%]	0.7 ± 0.2	2 ± 0.5	2 ± 0.5

Bonding without Pre and Post Heating

The conventional bonding process consists of several stages of heating and ultrasonic vibration which result in the morphology presented in Figs. 2–10. It is normally assumed that the initial intermetallic region is formed by diffusion in the solid state, but both the morphology and the composition of the intermetallic region that are presented in this work do not fit conventional diffusional growth due to the high density of voids and the formation of high temperature intermetallics ($AlAu_4$ and Al_3Au_8). This raises the question whether the bonding process occurs at the nominal bonding temperature, or whether a rise in the temperature occurs with the application of the ultrasonic energy combined with the latent heat released during intermetallic formation.

The bonding process consists of three stages: preheating of the Al pad; the wire-bonding stage where the bond is formed by the application of ultrasonic and thermal energy; followed by post-heating which is designed to reduce residual stresses resulting from plastic deformation that occurs during the wire-bonding stage. The morphology that is presented in Figs. 2–10 is the result of the application of heating and thermosonic energy in the bonding *and* post-heating stages. In order to understand the mechanism responsible for the morphology of the bond, the influence of the post-heating stage has to be eliminated. Therefore, bonding

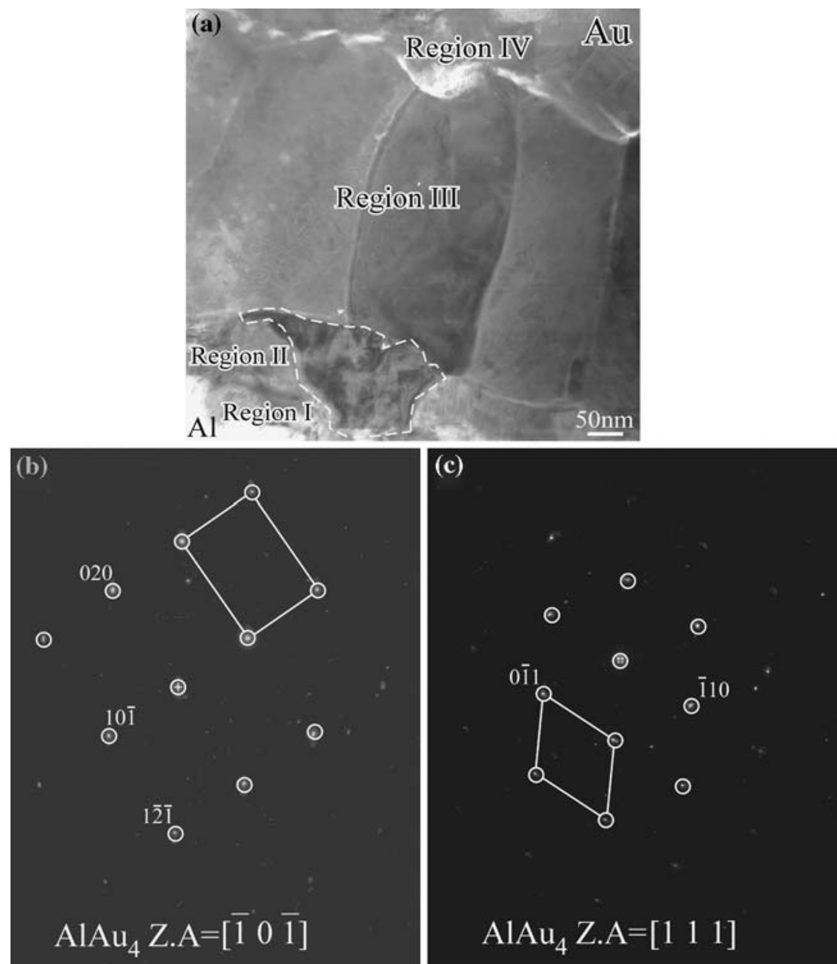

Fig. 10 (**a**) BF TEM micrograph of the intermetallic layer between a Au wire and a Al–1.0wt.%Si–0.5 wt%Cu pad. The two SADs in (**b**) and (**c**) confirm the existence of the metastable $AlAu_4$ cubic phase

of 5N Au wire to a Al-1.0wt.%Si pad was done, where the temperature of the pre and post-heating stage was room temperature and the bonding temperature was 165 °C (as in the previous samples). During the bonding stage the die is kept at the bonding temperature, which adds additional heating immediately subsequent to the bonding stage. In order to minimize this effect, the very last wire-bond that was joined on the die was analyzed.

Figure 11 is a HAADF STEM micrograph presenting the morphology of the bond after bonding *without* pre and post-heating, showing that during the application of ultrasonic and thermal energy a ~200 nm thick intermetallic region was formed. The intermetallic region contains a high density of flaws in the form of voids inside the intermetallic grains and at the grain boundaries. The morphology of the intermetallic region has the same four characteristic regions seen in the conventional wire-bonding process, where the elongated grains in region III are separated by a line of voids from region IV. According to this analysis the characteristic void-line that is present in the intermetallic region is formed in the short time (~140 ms) of the formation of the bond, and therefore can not be the

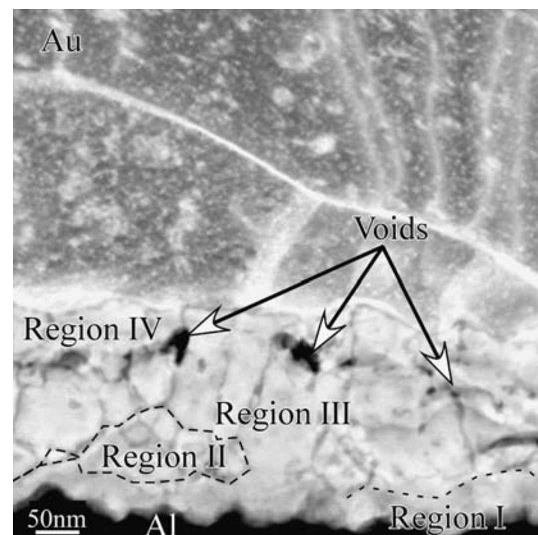

Fig. 11 HAADF HRSTEM micrograph of the Al–Au interface from a sample bonded without post-heating at a stage temperature of 165 °C

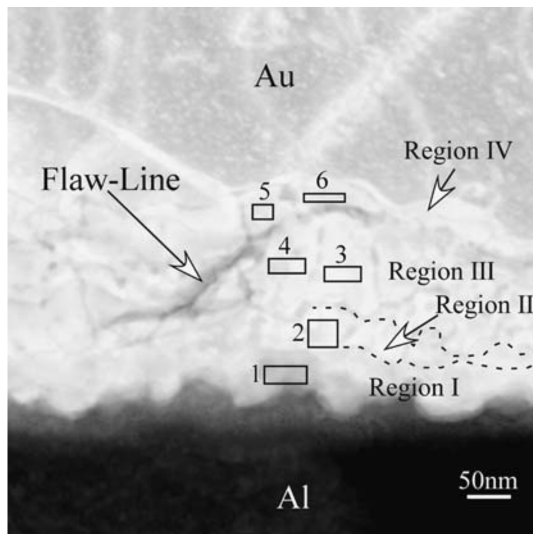

Fig. 12 HAADF HRSTEM micrograph of the intermetallic region from a sample bonded at 165 °C, without post annealing. EDS analysis was conducted from the indicated regions

Table 5 EDS results from areas 1–6 in Fig. 12

	1	2	3	4	5	6
Al (K) [at.%]	44 ± 9	20 ± 4	18 ± 4	18 ± 7	16 ± 3	16 ± 3
Au (L) [at.%]	51 ± 8	75 ± 11	76 ± 11	77 ± 11	78 ± 12	79 ± 12
Si (K) [at%]	5 ± 1	6 ± 1	6 ± 1	5 ± 1	6 ± 1	5 ± 1

result of long range diffusion processes such as void formation by the Kirkendall effect.

EDS analysis was conducted on the different areas indicated on the HAADF STEM micrograph in Fig. 12, and the results are summarized in Table 5. According to the EDS analysis Au rich intermetallics that contain Si are formed during the wire-bonding process. A comparison of the EDS results for the composition of the intermetallic region that is formed during the conventional wire-bonding process (Tables 1–3) show that almost no compositional changes occur during the post-heating stage, i.e. the intermetallics formed during the bonding stage continue to grow during the post heating stage.

The influence of bonding temperature on the formation of the intermetallic region

This work deals with the influence of temperature on the final morphology of the intermetallic region and the quality of the bond. Therefore a series of bonds was prepared in which no additional heating was applied (the same bonding parameters were used, optimized for 165 °C, throughout the test). The temperature of each die was set to a constant temperature, starting with room temperature (30 °C) up to 215 °C, while the temperatures of the pre and post bonding sites were kept at 30 °C. Sheer test and ball size measurements as a function of the die temperature were conducted on each sample. The results are presented in Figs. 13 and 14.

Figure 13 shows a direct relation between the ball diameter and the die temperature. This suggests that the die temperature increases the plastic deformation that occurs during bonding, and as a result the total contact area increases with bonding temperature.

The shear test results as a function of die temperature presented in Fig. 14 were derived from the measured load normalized by the measured bond area. The results show a direct relation between the bond strength and the temperature of the die. The normalized shear per area values for a pad temperature of 30

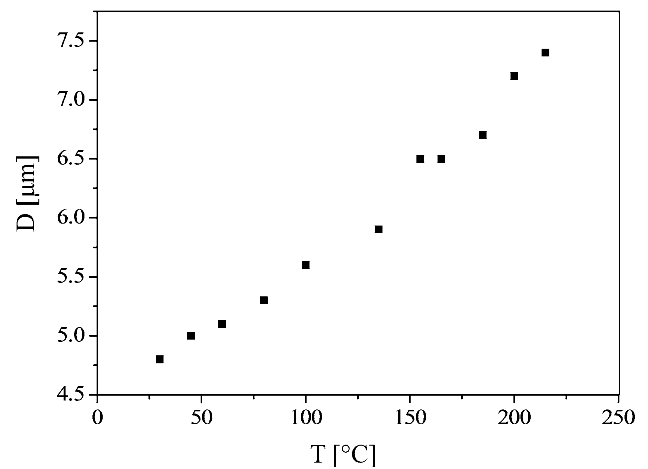

Fig. 13 Ball diameters as a function of die temperature

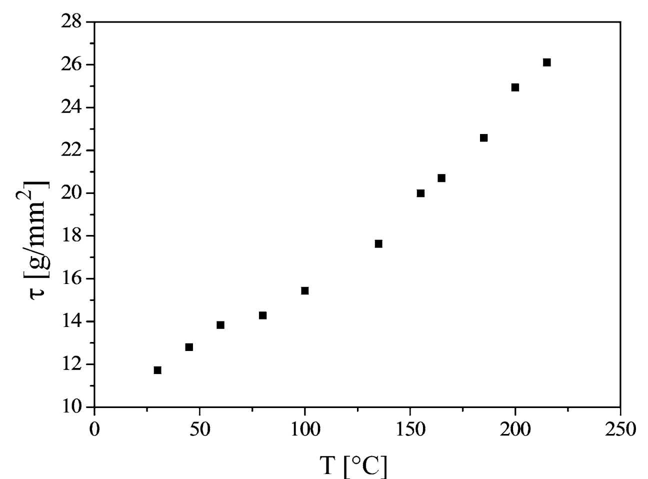

Fig. 14 Shear strength as a function of die temperature

and 215 °C were 11.7 and 26.1 g/mm^2, respectively. The strength of the bond increases due to the formation of the intermetallic region [1,2]. According to these results the die temperature also provides energy for Al–Au reaction in the bond region, which improves the bond strength. These results also prove that milliseconds of heating are enough for the formation of Al–Au intermetallics. Bonding at room temperature (30 °C) results in a low shear strength, which means that 120 kHz ultrasonic energy alone is insufficient for Al–Au bonding, and additional energy should be applied to form a bond at room temperature.

As presented in Fig. 11, during the application of heat and ultrasonic energy an intermetallic region is formed at the interface between the Au ball and the Al pad. According to the shear tests presented in Fig. 14 the strength of the bond increases with increase of the bonding temperature. In order to understand the morphological changes as a function of die temperature, S/TEM-EDS analysis of a sample that was bonded at a die temperature of 80 °C was analyzed. Since during the bonding process the entire die is subjected to the bonding temperature, which can cause additional reactions between the Al pad and the Au ball subsequent to the bonding stage, a sample was prepared from the last bond formed on the die. The HAADF STEM micrograph in Fig. 15 presents the morphology of the interface region of this bond.

A non-uniform reaction between the Au and Al, accompanied by the formation of voids, is visible in Fig. 15. EDS analysis confirmed that the dark regions

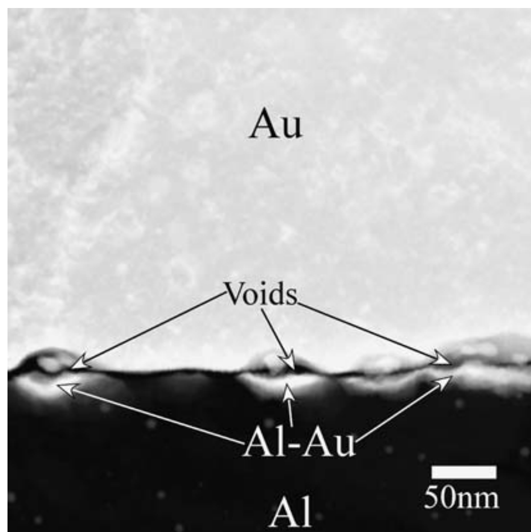

Fig. 15 HAADF HRSTEM micrograph of the Al–Au interface of a sample bonded without post-heating at a stage temperature of 80 °C, presenting voids in the Au adjacent to the thin Al–Au reaction region

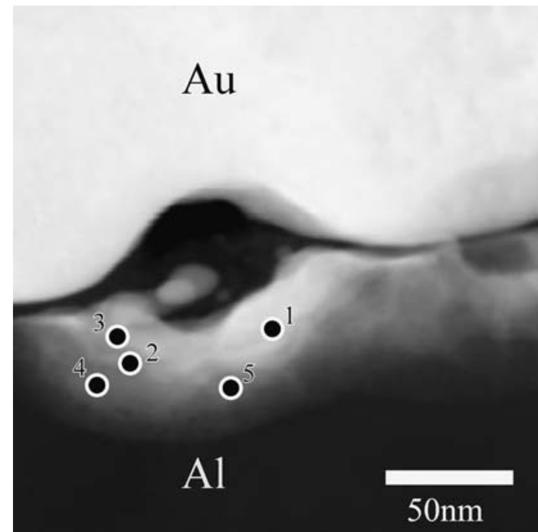

Fig. 16 HAADF HRSTEM micrograph of the Al–Au interface of a sample bonded without post-heating at a stage temperature of 80 °C. EDS analysis was conducted at the marked points

above the reaction regions in the Al are voids and not a region rich in Al. The bright contrast of the reacted region can be correlated with a large Au content in the HAADF STEM micrograph. Since the reaction is not uniform and the initial interface between the Au ball and the Al pad is visible, it can be concluded that the Al–Au reaction that occurred during the bonding process occurred within the Al pad, and as a result voids are formed in the Au, adjacent to the interface.

EDS analysis was conducted on the Al–Au region adjacent to a void. Figure 16 is a HAADF STEM micrograph of one of the voids at the interface. EDS measurements were conducted at the indicated points, and the results are summarized in Table 6.

The EDS results in Table 6 show a variation in the elemental concentration of the Al–Au region. Regions closer to the Al pad are richer with Al, and regions closer to the Au ball are richer with Au, which corroborates the change in contrast in the HAADF STEM micrograph in Fig. 16. According to these results a diffusion process occurs during the bonding stage which results in the formation of a Al–Au region with a composition gradient and local compositions exceeding the solubility of Al in Au or Au in Al [16].

Immediately prior to bonding, the free air ball is formed during a time interval of ~20–30 ms. As such,

Table 6 EDS results of points 1–5 in Fig. 16

	1	2	3	4	5
Al [at.%]	31 ± 6	54 ± 11	29 ± 6	78 ± 16	74 ± 15
Au [at.%]	96 ± 10	46 ± 8	71 ± 11	22 ± 5	26 ± 4

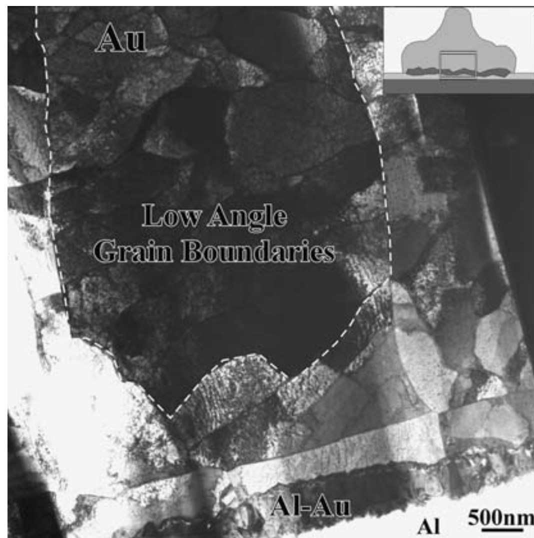

Fig. 17 BF TEM micrograph of the region indicated by the schematic drawing in the inset, presenting the Al–Au reaction region between the Al pad and the Au ball, and also the morphology of the gold ball. The region delimitated by the dashed line is a single Au grain, containing domains separated by low-angle grain boundaries

one must ask whether sufficient time elapsed between formation of the free air ball and the start of the bonding process to solidify the liquid Au. Figure 17 is a BF TEM micrograph of the Au ball bond after the bonding process, from the region indicated by the schematic drawing shown in the inset. The morphology in Fig. 17 includes flat Au grains adjacent to the intermetallic region, which contain a relatively high density of dislocations. In addition, sub-grains have formed inside the Au, suggesting that a recovery process occurs during bonding by dislocation movement to form low angle grain boundaries. The relatively high density of dislocation loops present in the Au grains is the result of radiation damage from the TEM sample preparation process [14]. The morphology of the Au region adjacent to the intermetallic region indicates that this region was plastically deformed *in the solid state* during the wire-bonding process.

Discussion

The Al–Au wire-bonding process is based on the fact that during the application of heat and ultrasonic energy a reaction between the Al pad and the Au ball occur which results in the formation of an Al–Au intermetallic region that forms a strong bond [1]. The temperature at which bonding occurs is lower than the melting point of both Al (660 °C) and Au (1064 °C) and therefore the bond is expected to form in the solid state by a diffusion reaction between the Al and the Au [1].

The influence of Si and Cu additions to the Al pad

The S/TEM-EDS results show that the content of the Al pad affects the formation of the Al–Au intermetallics during the wire-bonding process. The addition of Cu and Si to the Al pad significantly affects the morphology and uniformity of the intermetallic region. Therefore, the formation and growth of the intermetallic region depends on the dopants that are added to the commercial wires and pads, and intermetallic formation can not be predicted by simple examination of the binary phase diagrams.

EDS analysis of wire-bonds between 5N Au wire and Al–1.0wt.%Si–0.5wt.%Cu pads indicate a higher Au content in the Al–Au intermetallic region in comparison to intermetallics formed between a 5N Au wire and a Al-1.0wt.%Si pad. SAD studies of an intermetallic grain that contains Si and Cu confirm the structure of a metastable cubic form of $AlAu_4$. This means that the presence of Cu and Si, in addition to the non-equilibrium cooling rates inherent to the wire-bonding process, may stabilize metastable intermetallics. Additions of Cu to the Al pad results not only in a non-uniform intermetallic coverage of the interface, but also in a different crystallographic structure of the intermetallic region. This is also expected to affect the formation and growth of the intermetallic region during the life-time of the device.

Intermetallic formation as a function of the bonding conditions

The intermetallic region that is formed under conventional bonding conditions contains a high density of flaws in the intermetallic grains and at the grain boundaries. A characteristic flaw-line (void-line) is usually present between two regions with different morphologies, indicated as regions III and IV in Figs. 2, 3 and 8. In order to understand whether the source of these flaws is a diffusion process or local reduction of volume due to the formation of intermetallics, a bond that was subjected to temperature only during the wire-bonding stage was characterized. This bond contained the same characteristic flaws that are present in the intermetallic region of a conventionally bonded sample. The time for a complete bond is ~140 ms which does not permit long range diffusion processes to occur (such as void formation by the Kirkendall effect). Therefore it can be understood that the flaws that are formed inside the intermetallic

region are the result of volume changes due to the formation of the Al–Au intermetallics. The morphology of wire-bonds that were not subjected to heating beyond the ball-bonding stage includes a characteristic flaw line, formed during the bonding stage, which continues to grow during the application of temperature at the post-heating stage.

Analysis of the shear strength of the bond as a function of bonding temperature showed that an increase of the bonding temperature results in an increase of the bond strength, which according to the STEM analysis results from the growth of the intermetallic region. This correlates with conventional wisdom that the bond strength results from the amount of the intermetallics that are formed at the Al–Au interface [1, 2]. A comparison between wire-bonds bonded at 165 and 80 °C showed that at lower temperatures the transformation to Al–Au intermetallics occurs only in the Al pad, and the formation of intermetallics was accompanied by the formation of voids in the Au ball. Since the bonding time does not permit long range diffusion and condensation of vacancies by the Kirkendall effect which results in voids, void formation during the wire-bonding process must result from volume changes during intermetallic formation.

In order to understand the change in volume during intermetallic formation, the amount of volume that the atoms occupy in the lattice was calculated by the atomic packing factor (A.P.F) of Al, Au, Al_3Au_8 and $AlAu_4$. Table 7 presents the density and A.P.F of the pure metals and intermetallics that are formed at the bond interface. Al and Au are face centered cubic (FCC) metals with the highest packing density. Transformation of the pure metals to Al–Au intermetallics with a lower A.P.F. results in an increase in volume. In this case if the transformation of the pure metals to the intermetallics occurs in the solid state, it will not result in a reduction of volume as other studies suggested [2, 17]. This raises the question whether the transformation to the intermetallics occurs in the solid state, following conventional wisdom [1], or rather an increase in the temperature occurs during the bonding process, resulting in local melting at the interface region during the bonding stage.

Table 7 The density [17] and A.P.F of Al, Au and the intermetallics formed during annealing

	Density [g/cm^3]	A.P.F
Au	19.33	0.74
Al	2.7	0.74
$AlAu_4$	16.52	0.25
Al_2Au_5 (Al_3Au_8)	14.94	0.72

Since in the case of wire-bonding at 80 °C intermetallics were formed only in the Al pad, a calculation of the time that is needed for the formation of the intermetallic region by diffusion at various temperatures can be done using the semi-infinite rode approximation (Eq. 1), which can correlate between the time that is needed to form a Au-rich region inside the Al pad at various temperatures *in the solid state*. Taking into account the error in the EDS analysis, the finite atomic concentration of the Au in the Al pad was set to $C = 0.6$ (at $x = 0$, $C_0 = 1$). According to the EDS analysis the length of the intermetallic region where the concentration does not change was set to $x = 20$ nm. The diffusion coefficient for each temperature was calculated from Eq. 2 and data from the literature [18]. The diffusion time was extracted from equation 1 and estimated according to the characteristic diffusion length $x = \sqrt{Dt}$. According to these results (Table 8), the time for the formation of the intermetallic region at the bonding temperature and *in the solid state* is orders of magnitude beyond the actual process time.

$$C_x = C_0\left(1 - erf\left(\frac{x}{2\sqrt{Dt}}\right)\right) \tag{1}$$

$$D = 0.025\exp\left(-\frac{164.3\cdot 10^3}{RT}\right) + 0.83\exp\left(-\frac{212.3\cdot 10^3}{RT}\right) \tag{2}$$

Previous studies have shown that a rise in the ultrasonic frequency during the wire-bonding process helps to form a bond at lower temperatures [19]. This means that ultrasonic energy may supply the activation energy required to raise the temperature at the interface region during the bonding stage to reach a liquid state. The bonding process consists of ultrasonic energy that generates phonon vibrations which can cause a local increase in temperature. The presence of

Table 8 The time needed for the formation of a 20 nm region containing 60at.% Au inside the *solid* Al, as a function of the temperature

T [°C]	D[cm^2/sec]	$t = \frac{x^2}{D}$	$t_{(eq.\ 1)}$
80	1.22×10^{-26}	1.04×10^7 years	1.81×10^7 years
165	6.36×10^{-22}	200 years	346 years
175	1.74×10^{-21}	70 years	126 years
300	2.63×10^{-17}	42 h	3 days
400	4.45×10^{-15}	15 min	36 min
500	2.01×10^{-13}	20 s	35 s
600	3.85×10^{-12}	1 s	1.9 s
660	1.69×10^{-11}	0.8 s	0.4 s

impurities and defects in the lattice can add to phonon generation, and therefore increase the temperature at the interface during the bonding process [19]. A local increase of the temperature during the ball-bonding stage could conceivably result in a solid–liquid transition, and upon solidification flaws in the form of voids could form.

If a liquid state occurs at the interface region during the bonding stage, shrinkage will occur upon solidification, which can result in the formation of voids at the interface. For a solid-liquid transformation the solidification rate depends on the heat conductivity of the metals. The conductivities of Al, Au and the intermetallics are different [1], therefore upon solidification the regions that are adjacent to the Au and Al (region II and IV) should be the first to solidify. The elongated grains in region III suggest that the solidification time for this region is longer. Therefore, volume changes that occur during the solidification process of region III result in solidification voids. The morphology of region I corresponds to a diffusion gradient inside the Al that occurs during formation of the Al–Au intermetallic region and the subsequent solidification process.

When bonding occurs in a liquid state, flaws in the form of cavities and small voids in the intermetallic grains and at grain boundaries can be formed during the solidification process due to the reduction in volume and the capture of gas in the liquid. This can explain the high density of flaws found in the interface region of the bond.

Summary & conclusions

The wire-bonding process consists of ultrasonic and thermal energies that result in the formation of an intermetallic region which helps in forming a strong bond. S/TEM-EDS analysis showed that the morphology and uniformity of the interface depends on the content of the Al pad. Shear tests of samples bonded at various die temperatures showed a linear connection between the temperature and the strength of the bond. S/TEM analysis showed that during the bonding stage, ultrasonic and thermal activation can result in the formation of a liquid state at the bond interface. Upon solidification of the intermetallic region shrinkage occurs, which results in solidification voids.

According to the S/TEM-EDS results it is concluded that a correlation between the binary Al-Au phase diagram and the processes that occur during the bonding stage is incorrect due to the presence of dopants from the Al pad in the intermetallics and the cooling rate of the system that results in non equilibrium solidification.

Shear tests have shown that the bond strength results from intermetallic formation at the bond interface that forms by the application of *both* thermal and ultrasonic energies which cause a rise in the temperature. In addition to intermetallics that strengthen the bond, voids are formed. Simple elimination of the void-line by reducing the process temperature will result in a reduction of the bond strength due to insufficient intermetallic coverage at the interface.

The void-line is considered a main source for failure by cracks during the life time of the device. Additional work on the role of the void-line in failure that occurs during the life-time of the device has been conducted, and is presented in a companion paper (Karpel et al. in press, J Mater Sci, 2007) where it is shown that exposure to elevated temperatures results in crack formation at the intermetallic-Au interface, and not as a result from growth of the void-line.

It is concluded that bonding parameters, such as the die temperature and the post heating conditions, play and important role in the microstructural evolution that occurs during the life-time of the device, and careful consideration of the thermal activation provided by the ultrasonic vibration and die temperature has to be taken into account when bonding parameters are selected.

Acknowledgements The authors thank the Russell Berrie Nanotechnology Institute at the Technion for use of the dual-beam FIB, and I. Popov for assistance with use of the TEM.

Appendix

	Structure Type	Pearson symbol	Space Group	Lattice Parameters [nm]
Al_3Au_8 [15]	Al_3Au_8	*hR44*	$R\bar{3}c$	$a = 0.7724$ $c = 4.2083$
$AlAu_4$ [15]	W	*cI2*	$Im\bar{3}m$	$a = 0.324$

References

1. Harman G (1997) Wire-bonding in microelectronics materials process reliability and yield. McGraw-Hill Publishers
2. Noolu NJ, Murdeshwar NM, Ely KJ, Lippold JC, Baeslack WA (2004) J Mater Res 19(5):1374
3. Breach CD, Wulff F (2004) Microelectron Reliabil 44(6):973
4. Koeninger V, Uchida HH, Fromm E (1995) IEEE Trans Comp Pack Manufact Technol Part A 18(4):835
5. Chang HS, Hsieh KC, Martens T, Yang A (2004) IEEE Trans Comp Pack Technol 27(1):155

6. Maiocco L, Smyers D, Kadiyala S, Baker I (1990) Mater Character 24(4):293
7. Rooney DT, Schurr KG, Northrup MR (1996) Evaluation of wire quality by SEM analysis of ball-shape and visual inspection of intermetallic formation, ISHM 96 Proceedings: 432–433
8. Philofsky E (1970) Solid-State Electron 13(10):1391
9. Ueno H (1992) Mater Trans, JIM 33(11):1046
10. Breach CD, Tok CW, Wulff F, Calpito D (2004) J Mater Sci 39(19):6125
11. Williams DB, Carter BC (1996) Transmission electron microscopy. Plenum, New York
12. Reyntjens S, Puers R (2001) J Micromech Microeng 11(4):287
13. Clatterbaugh GV, Weiner JA, Charles HK (1984) IEEE Trans Comp Hybrid Manufact Technol 7(4):349
14. Bowden P, Brandon DG (1963) J Nucl Mater 9(3):348–354
15. Villars P (1991) Pearson's handbook of crystallographic data for intermetallic phases, 2nd edn, Vol. 1. ASM International, Materials Park, Ohio, pp 652–653
16. Okomoto H (1991) J Phase Equilib 12(1):114–115
17. Zhang X, Yan TT (2006). Thin solid films, proceedings of the international conference on materials for advanced technologies (ICMAT 2005) Symposium H: silicon microelectronics: processing to packaging—ICMAT 2005 Symposium H, 504(1–2):355–361
18. Smithells CJ (1992) Smithells metals reference book, 7th edn. Butterworth-Heinemann, Oxford
19. Ramsey TH, Alfaro C (1997) Semiconductor Int 20(9):93–94, 96